*Molecular Vision* 2005; 11:11-27 <http://www.molvis.org/molvis/v11/a2>
Received June 16 2004 | Accepted 6 December 2004 | Published 13 January 2005



# Detailed histopathologic characterization of the retinopathy, globe enlarged (*rge*/*rge*) chick phenotype

**Fabiano Montiani-Ferreira,[1] Andy Fischer,[2] Rafael Cernuda-Cernuda,[3] Matti Kiupel,[4] Willem Johan DeGrip,[5] David Sherry,[6] Sa Sun Cho,[7] Gillian C. Shaw,[1] Mark G. Evans,[8] Paul M. Hocking,[9] Simon M. Petersen-Jones[1]**

*[1]Department of Small Animal Clinical Sciences and [4]Diagnostic Center for Population and Animal Health, College of Veterinary Medicine, Michigan State University, East Lansing, MI; [2]Department of Neuroscience, Ohio State University, Columbus, OH; [3]Department of Morphology and Cellular Biology, University of Oviedo, Spain; [5]Department of Biochemistry, NCMLS, University of Nijmegen, The Netherlands; [6]College of Optometry, University of Houston, Houston, TX; [7]Department of Anatomy, Seoul National University College of Medicine, Seoul, Korea; [8]Pfizer Global Research and Development, Pfizer, Inc., Ann Arbor, MI; [9]Roslin Institute, Edinburgh, UK*

**Purpose:** The purpose of this study was to characterize the morphological abnormalities in the retinas of chicks (*Gallus gallus*) suffering from the autosomal recessive disease, retinopathy, globe enlarged (*rge*/*rge*).

**Methods:** *rge*/*rge* affected and age matched control retinas were examined from hatch up to 730 days of age. Thickness of retinal layers at six retinal regions was measured from plastic embedded sections. Morphological features were examined on semi-thin sections by light microscopy and on ultra-thin sections by transmission electron microscopy. Immunohistochemistry was performed using a panel of several different antibodies. Additionally, comparative counting of rod outer segments, rows of cells in the inner nuclear layer, and ganglion cells per unit length was performed.

**Results:** The earliest changes observed in *rge*/*rge* retinas were disorganization of the outer plexiform layer and abnormal location of the endoplasmic reticulum of the photoreceptors. In *rge*/*rge* retinas, cone pedicles were larger, irregular in shape, and usually contained multivesicular bodies. In addition, synaptic ribbons of the cone pedicles and rod spherules in *rge*/*rge* retinas were less numerous compared to controls. Large glycogen deposits progressively accumulated in the perinuclear cytoplasm associated with the abnormally located endoplasmic reticuli in accessory cones and rods. Total retinal thickness progressively decreased with age in *rge*/*rge* birds. This was accompanied by a decrease in the number of cells in the inner nuclear layer and a decrease in the number of rod outer segments (OSs). Several changes were detected in the *rge*/*rge* retinas using immunohistochemistry, including mislocalized opsin immunoreactivity of rod photoreceptors, a decrease in number and disorganization of opsin positive rod OSs (especially in the peripheral regions), a decrease in number of tyrosine hydroxylase positive neurites in the distal inner plexiform layer, and activation of macroglial and microglial cells.

**Conclusions:** As we previously reported, the *rge*/*rge* chick has vision loss that is not the result of photoreceptor loss and is unusual in that electroretinographic responses, although abnormal, are maintained until well after vision loss has developed. The phenotype is associated with a developmental disruption of both rod and cone photoreceptor synaptic terminals that progresses with age. It is possible that these changes may be indicative of abnormal circuitry within the outer plexiform layer, and that they underlie the progressive loss of vision in *rge*/*rge* birds. Other early changes suggesting photoreceptor abnormality are dilation of photoreceptor cell bodies, abnormal positioning of endoplasmic reticulum in the perinuclear region that is associated with abnormal glycogen deposition, and mislocalization of opsin immunoreactivity in rods. The *rge*/*rge* birds develop globe enlargement after the morphological and electroretinographic abnormalities. Globe enlargement in chicks can be induced by a number of different environmental factors. It is possible that abnormal signaling of photoreceptors to inner retinal cells could induce excessive ocular growth in the *rge*/*rge* birds. Many of the morphological changes such as retinal thinning seen in older *rge*/*rge* birds may be partly the result of the considerable globe enlargement that occurs later in the disease process. Molecular genetic studies to identify the causal gene mutation should help explain the morphological features of the *rge*/*rge* phenotype and clarify their association with vision loss and electroretinographic abnormalities.

Naturally occurring inherited retinal dystrophies in laboratory and domestic animals are valuable models of the human analogues. Phenotypically, they can be divided into different categories. For example, in some forms there is a failure in phototransduction resulting in a lack of development of normal retinal function, as assessed by electroretinography (ERG), followed by rapid loss of photoreceptors (e.g., *rd1* mouse, *rcd1* dog, and *rcd3* dog) [1-6]. Other gene mutations result in a progressive loss of photoreceptors, which up until their death, function relatively normally. Photoreceptor loss is reflected in a progressive reduction in ERG amplitudes (e.g., *prcd* dog) [7-9]. Some gene mutations result in a profound abnormality in retinal function as shown by vision testing and ERG testing and yet they have either no obvious retinal de-

Correspondence to: Simon M. Petersen-Jones, Department of Small Animal Clinical Sciences, Michigan State University, D-208 Veterinary Medical Center, East Lansing, MI, 48824; Phone: (517) 353-3278; FAX: (517) 355-5164; email: peter315@cvm.msu.edu

generation or just a slow retinal degeneration. Examples include congenital stationary night blindness where rod function is severely affected and yet the retina does not degenerate (e.g., *nob* mouse) [10] and mutations in RPE65 where rod and cone vision is severely affected and the ERG responses are grossly abnormal, and yet there is only a slow degeneration of the retina [11].

Chicken models of retinal dystrophy include the retinal degeneration (*rd*) chicken, which is due to a null mutation in photoreceptor guanylate cyclase [12]. Affected birds exhibit a severe phenotype with a lack of functional vision and nonrecordable ERG responses at hatch and a rapid retinal degeneration. The retinal dysplasia and degeneration (*rdd*) and blindness enlarged globe (*beg*) chicken also have phenotypes with loss of function and rapid development of structural retinal changes [13,14].

The retinopathy, globe enlarged (*rge*/*rge*) phenotype is a naturally occurring autosomal recessive form of blindness [15,16]. Linkage analysis maps the *rge*/*rge* locus to chicken chromosome 1 [17]. There is a variable degree of vision loss in *rge*/*rge* chicks at 1 day of age with deterioration in vision over the next few weeks until all chicks are unable to see food particles on the floor and behaviorally act as if they are blind [18]. However, optokinetic responses can still be induced in some birds until several months of age [18]. The affected birds develop globe enlargement, which is apparently secondary to the vision loss [17,18]. Preliminary ERG studies show that *rge*/*rge* chicks have an elevated response threshold, a decrease in oscillatory potentials, and interestingly, a supernormal b-wave amplitude in response to brighter flashes [18].

Supernormal ERG responses have been described in other retinopathies such as enhanced S cone syndrome [19,20] and Best's macular dystrophy [21]. The *rge*/*rge* chicken phenotype is unusual in that the ERG, although abnormal from initial development, only slowly deteriorates and is maintained for several months after functional vision loss. Another unusual feature is that on examining the retina by routine light microscopy, no gross structural abnormalities were apparent initially and there was only a slow progressive thinning of retinal layers apparent after the age of functional vision loss [18]. Therefore, in the *rge*/*rge* chicks, loss of vision does not appear to correlate directly with a loss of photoreceptor function (as assessed by the ERG) nor with a loss of photoreceptor cells.

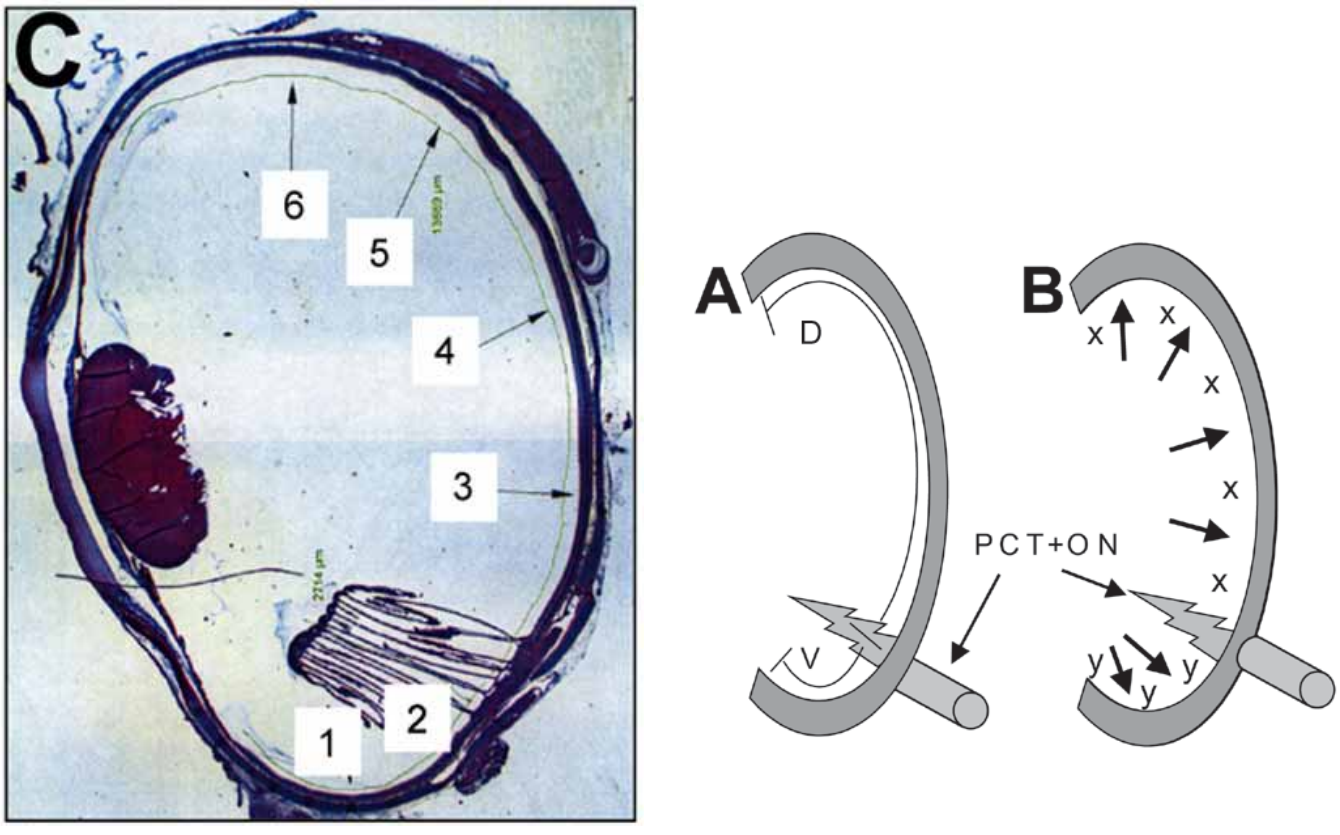


Figure 1. Selection of regions for retinal thickness measurement. Graphical representation of the method used for determining the retinal regions used for retinal thickness measurement. **A**: Measurements were made of retinal length from the ora serrata; dorsal (D) and ventral (V) to the pecten/optic nerve (PCT+ON). **B**: The value D was divided by 5, resulting in x and the value V was divided by 3, resulting in y. Starting at the center of PCT+ON, x and y values (dorsally and ventrally, respectively) were consecutively applied to determine the regions to be evaluated for retinal thickness. **C**: Cross section of a chick eye globe showing the 6 positions at which retinal thickness measurements were made.

The purpose of the study reported here was to examine the histopathological changes in the retina of the *rge*/*rge* birds in more detail by light microscopy (LM), immunohistochemistry (IHC), and electron microscopy (EM).

## METHODS

*Animals:* A flock of *rge*/*rge* birds was bred to produce homozygous affected (*rge*/*rge*), heterozygous carrier (*rge*/+) and homozygous normal (+/+) chicks. Progeny from *rge*/*rge* crossed with *rge*/+ birds were phenotyped by ERG, as described previously [18]. Birds were kept under standard lighting conditions with a 12:12 h light-dark cycle with ad libitum access to a commercial chicken diet (Home Fresh Poultry Feed, Kent Feeds, Muscatine, IA). All experiments and procedures were carried out in accordance with the ARVO Statement for the Use of Animals in Ophthalmic and Vision Research and approved by the Institutional Animal Use Committee.

Immediately following euthanasia using a $CO_2$ chamber, bilateral enucleation was performed. The eyes were hemisected at the equator, the vitreous body removed and the posterior segment of the eye immersed into one of the different types of fixatives used (see below). Samples from control and *rge*/*rge* birds were studied at several different ages.

*Morphometric analysis:* Retinal thickness was measured on plastic embedded histological sections (Immunobed, Polysciences, Warminster, PA) at 6 consistent points across the retina (Figure 1). The retinal regions analyzed were defined by measuring the ventral and dorsal retinal lengths from pecten to ora serrata under 10x magnification (Figure 1A) using the software SPOT version 3.5 for windows (Visitron Systems, Gmbh, Puchheim, Germany). The distance from pecten to ora serrata was divided by 3 (ventral) or 5 (dorsal; Figure 1B) to give the 6 locations for measurement of retinal thickness (Figure 1C). Digital images were acquired under 400x magnification and stored using the same software. Subsequently, Image Pro Plus version 4 (IP4) software (Media Cybernetics, Silver Spring, MD) was used to measure the histological thickness of 7 retinal layers defined as: nerve fiber layer (NFL) and ganglion cell layer (GCL); inner plexiform layer (IPL); inner nuclear layer (INL); outer plexiform layer (OPL); outer nuclear layer (ONL); photoreceptor inner segment (IS) and outer segment layer (OS); and retinal pigment epithelium (RPE). Total retinal thickness was also measured at each of the six points. Care was taken to ensure that the sections were oriented perpendicular to the retinal surface.

Using paraffin embedded sections labeled with rhodopsin antibody (see details of the staining technique below), rod OSs were manually counted in 200 μm segments of retinal length, using the same 6 regions described above. Additionally, the numbers of rows of cells in the INL, at each region, and the number of ganglion cells per 200 μm at each of the same 6 retinal regions were measured. The number of rows of nuclei in the ONL is commonly used as a parameter of photoreceptor cell density in histological studies of retinal degeneration in other species [22]. In the case of birds, the ONL is a bilayered nuclei row, with rod nuclei located more internally than cone nuclei and therefore counting the number of rows of nuclei would not be a sensitive measure of photoreceptor density.

Statistical analyses for retinal thickness measurements, number of rod outer segments, ganglion cells per unit length, and for the number of rows in the INL were performed by one way ANOVA and t test (when comparing one time point between two groups). The tests were run using two different statistical analysis software packages (StatView version 5.0, SAS Institute, Cary, NC; SAS Version 8.2, SAS Institute, Cary, NC). If any statistically significant difference was found, the data were further analyzed using post hoc comparisons with Fisher's or a Tukey-Kramer test. Data were deemed significant when p values were less than 0.05.

*Conventional morphologic analysis of semi-thin and ultra-thin sections:* The eyecups were fixed in phosphate buffered (0.1 M, pH 7.3), 3% paraformaldehyde, 2% glutaraldehyde solution for 3 h at room temperature. A square shaped tissue sample (about 2x2 mm) per eye was collected from the central retina, subsequently post-fixed in 1% $OsO_4$ at 4 °C for 2 h, washed in distilled water, then dehydrated in acetone and finally embedded in an Araldite based resin (Durcupan, Fluka, Seelze, Germany) or, sometimes, in plastic (Immunobed, Polysciences, Warminster, PA). Semi-thin (0.5-1 μm) and ultra-thin (80 nm) sections were cut using a Reichert-Jung ULTRACUT ultra-microtome (Reichert-Jung, Wien, Austria), using glass and diamond knives, respectively. Semi-thin sections were stained with toluidine blue solution and examined by light microscopy and images recorded with a Polaroid DMC digital camera (Polaroid, Waltham, MA) mounted on a Nikon Eclipse E400 Microscope (Nikon, Melville, NY). Ultra-thin sections were mounted on copper grids, stained with lead citrate and uranyl acetate, and examined and photographed in a Zeiss EM 109 transmission electron microscope (TEM; Carl Zeiss, Inc., Thornwood, NY). TEM photographic negative films were digitalized using a Polaroid SprintScan 35 Plus scanner (Polaroid, Waltham, MA).

A search for possible apoptotic nuclei was conducted using standard morphological criteria [23] utilizing both semi-thin and ultra-thin sections. These criteria include the presence of darkly stained nuclei (compact chromatin), which also are electron dense in ultra-thin sections, and the presence of pyknotic or fragmented nuclei (also called apoptotic bodies) [23].

*Examination for morphological features of apoptosis:* Despite close examination of sections from *rge*/*rge* retinas at several different ages by light and electron microscopy, no cells displaying morphological features that would indicate they were undergoing apoptosis were seen.

*Immunohistochemistry studies on paraffin embedded material and frozen sections:* For IHC analyses in paraffin embedded sections, retinal samples were fixed in 4% paraformaldehyde, 3% sucrose in 0.1 M phosphate buffer for 48 h at 4 °C and then dehydrated in ethanol and embedded in paraffin blocks prior to sectioning. 8 μm thick sections were cut and mounted on double gelatinized glass slides. After deparaffination in xylene, sections were rehydrated gradually in ethanol and distilled water. IHC analysis in paraffin was

carried out by single labeling with the following antisera: Mouse opsin monoclonal antibody at 1:1000 (Lab Vision, Fremont, CA), Rabbit anti-glial fibrilliary acidic protein (GFAP) at 1:2000 (Dako, Carpinteria, CA), Tyrosine hydroxylase at 1:1000 (Chemicon International, Temecula, CA), Guanylate cyclase activating protein (GCAP1) at 1:400 (a gift from Dr. Palczewski, University of Washington, Seattle, WA).

The peroxidase conjugated Vectastain ABC (avidin-biotin complex) kit (Vector, Burlingame, CA) was employed as a detection system. Labeled sections were dehydrated in ethanol, cleared in xylene, mounted in a hydrophobic medium

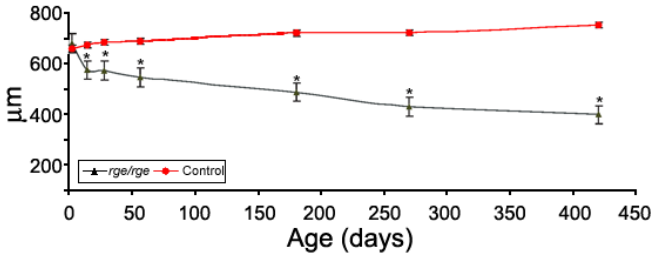


Figure 2. Total retinal thickness comparison. Total retinal thickness of *rge*/*rge* (black line) and control birds (red line) at 2, 14, 28, 56, 180, 270, and 420 days of age. Note that the mean retinal thickness decreases with age in the *rge*/*rge* group. By 14 days of age, the retinal thickness of *rge*/*rge* chicks was significantly thinner than that of controls (574.5±13.5 µm compared to 672.8±11.4 µm; 4 in each group; asterisk indicates p<0.05).

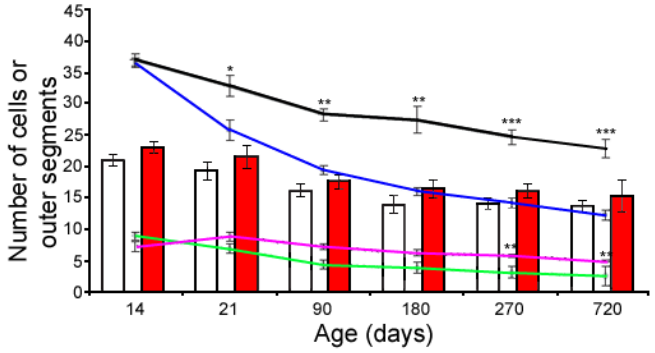


Figure 4. Retinal cell counting. Number of rod OSs and ganglion cells per unit length and number of rows in the INL (average of the six retinal regions demonstrated in Figure 1) in cross sections at 14, 21, 90, 180, 270, and 720 days of age. Note the progressive and significant (p<0.01) overall decrease in number of rod OSs per 200 µm of retinal length in the *rge*/*rge* retinas (compare black control line with blue line). At 21 days of age the difference was significant. Additionally, the mean number of rows of nuclei in the INL became significantly smaller in the *rge*/*rge* group (compare pink control line to green*rge*/*rge* line) at 270 days of age (p<0.0001; 4 *rge*/*rge*, 3 controls). The mean number of ganglion cells per 200 µm of retinal length was not statistically significant between the two groups (compare red control columns to white *rge*/*rge* columns). A mean number of 4 retinal samples from *rge*/*rge* and control birds were analyzed from each age group. Asterisks indicate significance. The single asterisk indicates p<0.01, the double asterisks indicates p<0.001, and the triple asterisks indicates p<0.0001.

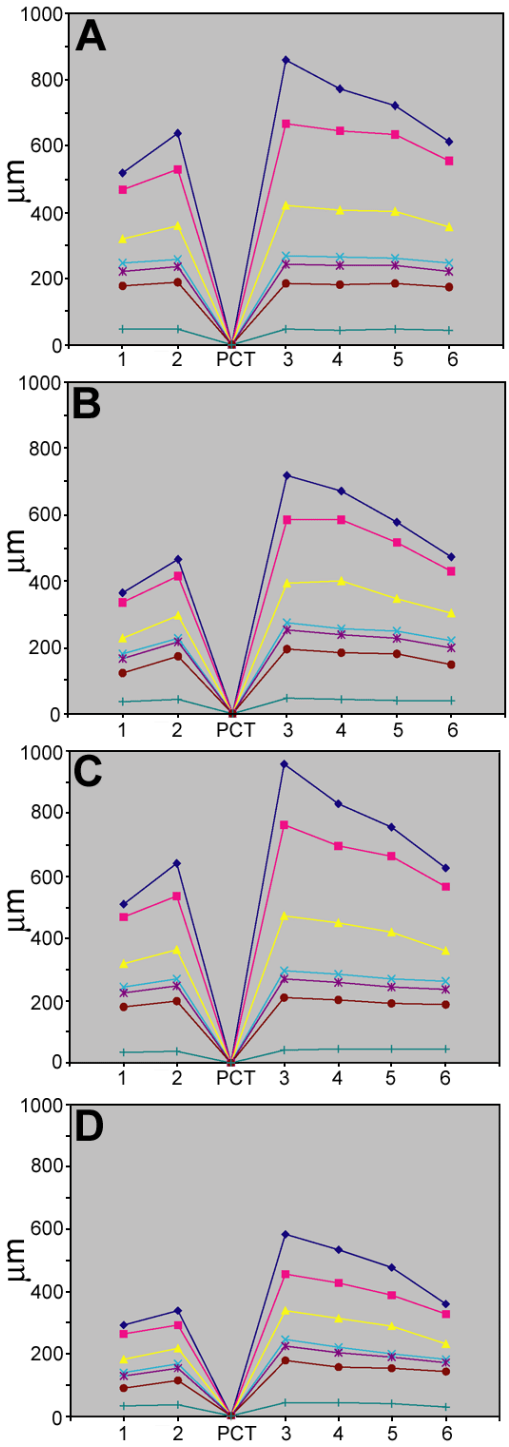


Figure 3. Regional retinal thickness comparison. Mean retinal thickness of each of the different retinal layers from *rge*/*rge* (**B**,**D**) and control (**A**,**C**) birds at two representative age groups. By 56 days of age (**A**,**B**; 6 *rge*/*rge*, 4 controls), mean thickness of NFL plus GCL (blue), IPL (pink), INL (yellow) and also OS plus IS (brown) layer were already decreased. Note that the ventral regions (1 and 2) and the far dorsal peripheral region (6) thinned the most. In retinas from birds at 270 days of age (**C**,**D**; 4 *rge*/*rge*, 5 controls), the thickness of the NFL plus GCL, IPL and IS plus OS retinal layers was markedly decreased. The other colored lines represent the retinal pigment epithelium (aquamarine), outer nuclear layer (purple), outer plexiform layer (turquoise), and pecten (PCT).

(Entellan, Merck, Darmstadt, Germany) and examined by LM.

For IHC analyses in frozen sections, the retinal samples were immersed in 4% paraformaldehyde plus 3% sucrose in 0.1 M phosphate buffer, pH 7.4 or Carnoy fixative for 30 min at room temperature (for RCA-1). Fixed tissues were washed three times in phosphate buffered saline plus 0.05 M phosphate buffer and 195 mM NaCl, pH 7.4, (PBS), and cryoprotected in PBS plus 30% sucrose overnight at 4 °C. Cryoprotected tissues were soaked in embedding medium (O.C.T.-compound; Tissue-Tek, Sakura Finetek U.S.A., Inc., Torrance, CA) for 30 min and freeze mounted onto sectioning blocks. Vertical 14 μm thick sections were cut on a Reichart-Fridgocut™ 2500 (Reichert-Jung, Wien, Austria), and thaw mounted onto Super-Frost™ slides (Fisher Scientific, Suwanee, GA). Sections from control and *rge*/*rge* eyes were placed together in pairs on each slide to ensure equal exposure to reagents. Sections were air dried and stored at -20 °C until needed.

Sections were thawed at room temperature, ringed with grease, and washed two times in PBS. They were then covered with primary antibody solution (150 μl of antibody diluted in PBS, plus 0.3% Triton X-100 and 0.01% $NaN_3$) and incubated for about 24 h at room temperature in a humidified chamber. The slides were washed two times in PBS, covered with the secondary antibody solution and incubated for at least 1 h at room temperature in a humidified chamber. Finally, they were washed three times in PBS, and a coverslip was applied in 4:1 (v/v) glycerol to water.

Working dilutions and sources of antibodies used in frozen sections included the following: Mouse anti-lysosomal glycoprotein at 1:80 (LEP-100; Developmental Studies Hybridoma Bank, DSHB; Iowa City, IA), Rat anti-glycine at 1:1000 (a gift from Dr. D. Pow, University of Queensland), Rabbit anti-tyrosine kinase A (TrkA) at 1:5000 (a gift from Dr. F. Lefcort, Montana State University), Mouse anti-neurofilament at 1:2000 (RMO270; Zymed Laboratories, South San Francisco, CA), Mouse anti-vimentin 1:50 (H5; DSHB, Iowa City, IA), Mouse anti-Islet1 at 1:50 (39.4D5; DSHB, Iowa City, IA), Mouse anti-Hu at 1:200 (Monoclonal Antibody Facility, University of Oregon), Mouse anti-rhodopsin at 1:800 (rho4D2; a gift from Dr. R. Molday, University of British Columbia, Vancouver, Canada), Mouse anti-tyrosine hydroxylase at 1:100 (DSHB, Iowa City, IA), Rabbit anti-glial fibrilliary acidic protein (GFAP) at 1:2000 (Dako, Carpentaria, CA), Mouse anti-visinin at 1:100 (DSHB, Iowa City, IA), *Ricinus communis* agglutinin-1 (RCA-1; produced by one of the authors SSC), Tfbp-transferrin binding protein (TfBP; produced by SSC), Mouse anti-β3 tubulin at 1:2000 (TUJ-1; BabCO, Princeton, NJ), Calbindin D28 at 1:1000 (Sigma-Aldrich, St. Louis, MO), Mouse anti-glucagon at 1:400 (a gift

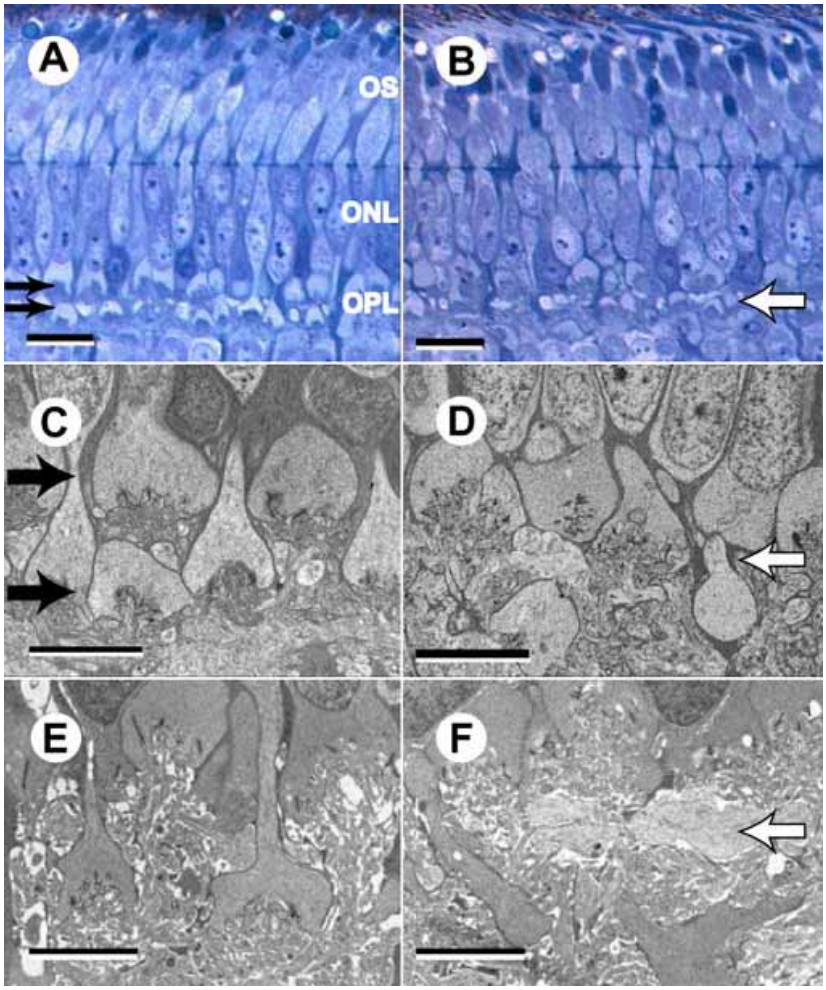


Figure 5. Morphological abnormalities of the outer plexiform layer. Semi-thin (**A**,**B**; toluidine blue) and ultra-thin (**C**,**D**) retinal sections of a control (**A**,**C**) and of an *rge*/*rge* chick (**B**,**D**), at 1 day of age. **E**,**F** are ultra-thin sections of a control (**E**) and an *rge*/*rge* chick (**F**), at 60 days of age. **A**: Semi-thin section of a control chick retina demonstrating the detail of the well organized outer OPL. The normal 2 layer arrangement of the photoreceptor synaptic terminals is indicated (two black arrows). **B**: Note the dilated photoreceptor cell bodies and the disorganization of the OPL architecture in the sample from an *rge*/*rge* chick (white arrow). **C**: The typical 2 layer arrangement of the photoreceptor synaptic terminals is clearly shown here (two black arrows). **D**: The two layer arrangement of the photoreceptor terminals is lost (white arrow); they were seen in **C** (two black arrows). Note the disruption of the photoreceptor pedicles and spherules. **E**,**F**: The two layer arrangement of the photoreceptor pedicles and spherules is even further disorganized (white arrow) in the *rge*/*rge* section compared to controls at 60 days of age. Note that there are fewer synaptic ribbons in the *rge*/*rge* section (**F**) compared to control (**E**) at this age. In **A**,**B**, the bars represent 10 μm. In **C**-**F**, the bars represent 5 μm. The outer segments (OS), outer nuclear layer (ONL), and outer plexiform layer (OPL) are labeled.

from Dr. M. Gregor, University of Tuebingen, Germany), Rabbit anti-caspase-3 at 1:1000 (R&D Systems, Minneapolis, MN), Rabbit anti-synaptobrevin (anti-VAMP-1) at 1:400-1:800 (Synaptic Systems, Goettingen, Germany), Mouse anti-synaptic vesicle protein 2 (SV2) at 1:25 (a gift from Dr. Kathleen Buckley, Harvard Medical School), Mouse anti-GABA-A receptor β subunit at 1:100-1:500 (clone 62-3G1; Upstate Biologicals, Charlottesville, VA).

Secondary antibodies for frozen or paraffin embedded sections included goat-anti-rabbit-Alexa568, goat-anti-mouse-Alexa568, goat-anti-mouse-Alexa488, goat-anti-rat-Alexa488 (Molecular Probes, Eugene, OR) and goat anti-mouse-Cy3 (Biomeda, Foster City, CA), diluted to 1:500 in PBS plus 0.3% Triton X-100.

Fluorescence photomicrographs were taken with a Ziess Axioplan II microscope (Carl Zeiss, Inc., Thornwood, NY) equipped with epifluorescence, FITC and rhodamine filter combinations, and a Spot™ Slider-RT digital camera (Diagnostic Instruments, Inc., Sterling Heights, MI). Images were optimized for color, brightness and contrast using (Adobe Photoshop 6.0, Adobe Systems, Mountain View, CA).

*Terminal deoxynucleotidyl transferase mediated dUTP nick end labeling (TUNEL) staining:* TUNEL staining was performed to identify cells undergoing apoptosis, following previously described techniques [24] in retinal sections from *rge*/*rge* and control birds at 13 and 30 days of age. In brief, slides were warmed to 20 °C and washed once in PBS, followed by one wash in PBS plus 0.3% Triton X-100, and two more washes in normal PBS. Sections were then covered with 100 µl of incubation medium (0.5 nmol Cy3 conjugated dCTP, 20 units of 38 terminal deoxynucleotidyl transferase [Amersham, Little Chalfont, United Kingdom], 100 mM sodium cacodylate, 2 mM Co $Cl_2$, and 0.25 mM β-mercaptoethanol in sterile saline, pH 7.2) and incubated for 1 h in a humidified chamber at 37 °C. The sections were then washed three times in PBS, mounted in 4:1 (v/v) glycerol to water, and coverslips were added for observation by epifluorescence with a rhodamine filter combination.

## RESULTS

No significant differences were observed between heterozygous carrier (*rge*/+) and homozygous normal (+/+) chicks on light and electron microscopy analysis or by immunohistochemistry techniques using several cell type specific markers (data not shown). For this reason carriers and normal retinas were considered interchangeably as controls in the sections presented here.

*Morphological measurements of the retina:* At two days of age there was no difference in retinal thickness of *rge*/*rge* chicks compared to controls, but by 14 days of age the *rge*/*rge* retinas were significantly thinner (574.5±13.5 µm compared to 672.8±11.4 µm, $p<0.05$; Figure 2). From this age point onwards, a slow thinning of the retina continued in the *rge*/*rge* birds. There was a geographic difference in the rate of thinning. The ventral regions (1 and 2 in Figure 3) and the far dorsal peripheral region (6 in Figure 3) had the greatest initial reduction in thickness (Figure 3B). At 14 days of age, the thickness (mean of all six retinal regions measured) of the NFL plus the GCL (109.8±48.7 µm compared to 175.2±9.4 µm), IPL (193.2±3.8 µm compared to 202.6±3.8 µm), and INL (177.5±3.6 µm compared to 190.3±3.8 µm) were significantly thinner ($p<0.0001$) in *rge*/*rge* birds than in controls. By 56 days of age, most retinal layers were significantly thinner ($p<0.001$) in the *rge*/*rge* birds, except the OPL, ONL, and RPE. The difference in the above mentioned layers became even greater in older birds (Figure 2, Figure 3). By 270 days of age all retinal layers with exception of the RPE of all six retinal regions were significantly thinner compared to controls ($p<0.0001$, Figure 3C,D).

A progressive and significant ($p<0.01$) overall decrease in the number of rod OSs per unit length of retina occurred in the *rge*/*rge* birds with age. By 21 days of age, the overall mean rod OS number in *rge*/*rge* retinas was significantly lower than controls (26.3 ± 5.1 compared to 33.3 ± 5.9 per 200 µm length of retina, $p<0.05$; Figure 4). Additionally, the mean number of nuclei rows of the INL in the *rge*/*rge* group decreased with age but only became significantly lower than controls by 270

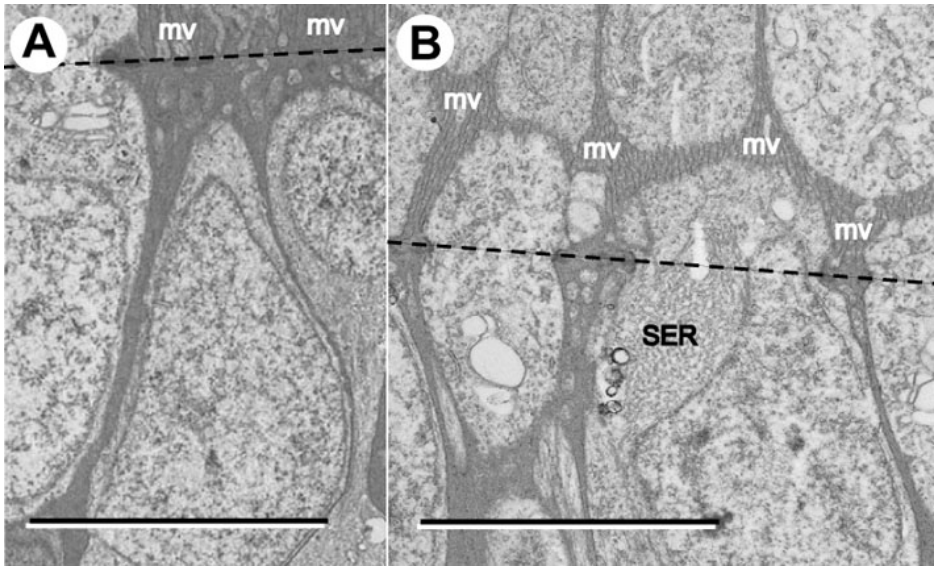


Figure 6. Displacement of smooth endoplasmic reticulum. Ultrastructural features of the ONL/IS interface of a control (**A**) and an *rge*/*rge* chick (**B**), at 1 day of age. **A**: Note the absence of endoplasmic reticulum in the perinuclear region. The bar represents 3.5 µm. **B**: Note the displacement of the smooth ER (marked as SER), which, in this sample, is located at the perinuclear cytoplasm of an accessory cone, internal to the level of the outer limiting membrane (dashed line). At this age accumulation of glycogen is not apparent (compare with Figure 7 and Figure 10). Müller cell microvilli are marked as "mv". The bar represents 5 µm.

days of age (3.0 ± 0.9 compared to 6.7 ± 1.6 per 200 μm length of retina, p=0.0058; Figure 4). The mean number of ganglion cells per unit length of retina of both *rge*/*rge* and controls tended to decrease with age, however there was no significant difference between *rge*/*rge* and control groups at the ages assessed (up to 720 days of age; Figure 4).

*Retinal sections of one day old chicks:* Semi-thin sections from *rge*/*rge* chicks at one day of age (Figure 5B) revealed that the basic morphological retinal features were similar to the controls (Figure 5A), although the cell bodies within the ONL of the *rge*/*rge* sections appeared consistently somewhat dilated and less fusiform shaped than in controls. However, the most striking difference was observed in the OPL. In the control chicks the photoreceptor terminals formed two distinct layers (Figure 5A,C). This regular stratification was not present in the *rge*/*rge* retinas (Figure 5B,D). Furthermore, the photoreceptor pedicles appeared to be distorted in *rge*/*rge* sections (compare Figure 5C,D). There also appeared to be an abnormal positioning of the endoplasmic reticulum (ER) in some photoreceptor cells of *rge*/*rge* birds. In control birds the ER, which contained some glycogen granules, was present in the ISs of rods (as part of the hyperboloid) and accessory cones (as part of the paraboloid) whereas in the *rge*/*rge* retinas the ER of the accessory cones were located internal to the outer limiting membrane, close to the nucleus (Figure 6).

*Retinal sections of seven day old chicks:* By seven days of age, the OPL of the *rge*/*rge* chicks was more disorganized than at one day of age (Figure 7A). At this point, photoreceptor pedicles and spherules were increased in size compared to controls (Figure 8A). These abnormally wide terminals were not as electron dense as those of controls and often contained sets of numerous flattened (tubuliform) small vesicles, and multivesicular bodies (Figure 8C). The number of synaptic ribbons observed in the cone pedicles and rod spherules also appeared to be reduced in all sections from *rge*/*rge* birds examined (data not shown). However within the IPL no apparent difference in the number of ribbons between *rge*/*rge* and controls was noted (data not shown). The organelles of the *rge*/*rge* photoreceptors also showed further changes. In control retinas the ISs of the accessory cells had well arranged smooth ER, with small glycogen granules present among the cisterns. There was a geometrical arrangement of the cisterns and a close relationship with the rough ER. By comparison, *rge*/*rge* retinas had larger glycogen deposits in the ISs of the accessory cells of double cones and also abnormally located deposits in the supranuclear cytoplasm (Figure 7A,B) and in the subnuclear cytoplasm close to the synaptic regions and associated with ER (Figure 7D). Increased prominence of electron dense glial processes around the photoreceptors could be observed at this age and at later stages, also (Figure 9 and Figure 10).

*Retinal sections of chicks between 60 and 90 days of age:* By 60 to 90 days of age the disruption of the OPL of *rge*/*rge* birds had progressed and the number of discernible synaptic

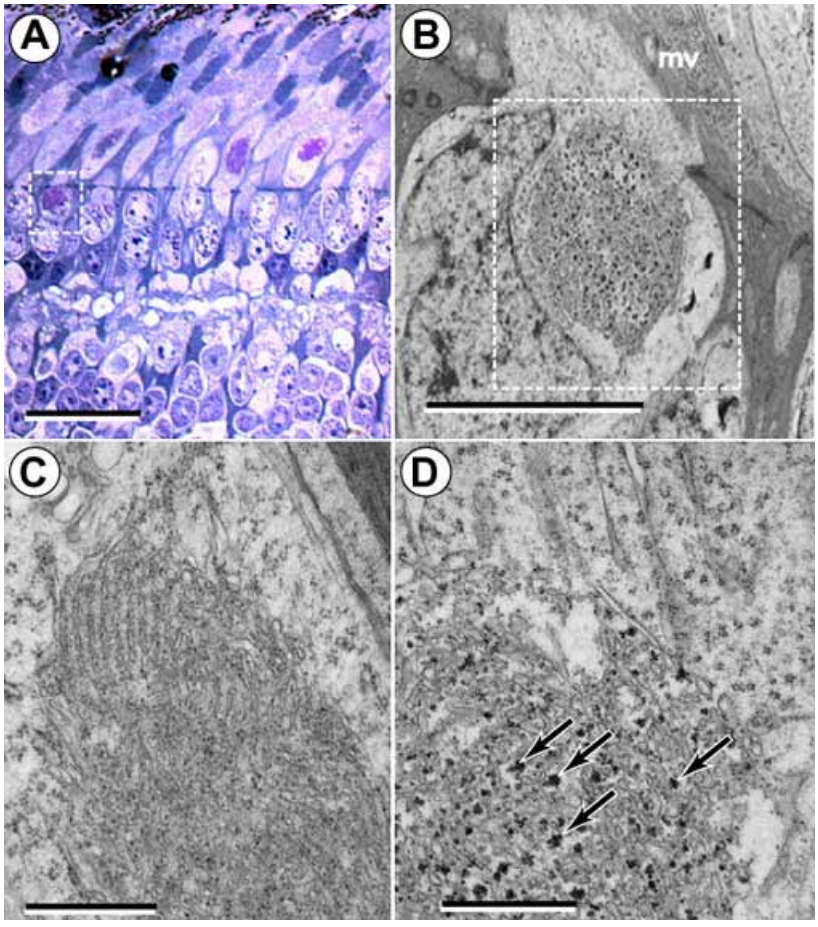


Figure 7. Mislocalization of glycogen deposits. Semi-thin (**A**) and ultra-thin (**B**,**C**,**D**) sections of *rge*/*rge* (**A**,**B**,**D**) and control (**C**) retina at 7 days of age. **A**: Semi-thin section showing the detail of a large glycogen deposit (dashed white square) in the perinuclear cytoplasm. Note the disrupted OPL. The bar represents 20 μm. **B**: Ultrastructural detail of a deposit in the perinuclear cytoplasm of an accessory cell of double cone of an *rge*/*rge* bird where it is possible to observe the abnormal accumulation of glycogen (dashed white square). The bar represents 5 μm. An electron dense glial process of a Müller cell (mv) located between the ISs of the photoreceptor cells is indicated. **C**: Control retina showing evenly arranged SER in the IS (paraboloid). Small glycogen granules can be seen among the cisterns. The bar represents 1 μm. **D**: Higher magnification of section in **B** to show abnormal accumulations of glycogen associated with ER (black arrows). The bar represents 1 μm.

ribbons in the OPL was also further decreased. As observed in younger *rge*/*rge* chicks, glycogen deposits were often displaced from the normal position in the IS towards the cytoplasmic perinuclear areas of the accessory cells of double cones and of the rod cells (Figure 9B). The glycogen deposits in rods of *rge*/*rge* birds were larger than those that could occasionally be seen in the rod ISs of control retinas. Some occasional whorls of membranes (myelinoid figures) could be seen in the rod cells, most commonly in the subnuclear cytoplasm (Figure 9C).

Large Müller cell processes were present in the OPL and occasionally separated the somata of the photoreceptor cells in *rge*/*rge* retinas. Abundant Müller cell processes and microvilli could also be seen among the ISs of the photoreceptor cells (Figure 9A).

*Retinal sections of 270 day old chicks:* By this age the retinal thickness of *rge*/*rge* birds was markedly decreased compared to controls (Figure 2; compare Figure 3C,D; compare Figure 10A,B). Both rod and cone photoreceptors could still be readily identified, although the OSs were considerably shorter (Figure 10B,C). The spaces between photoreceptors, which were occupied by Müller cell processes, were increased in size (Figure 10D). In addition, cone OSs appeared disorganized; they were shorter than controls with disruption of the discs (Figure 10C). The abnormal photoreceptor glycogen deposits were larger than at the other ages and often displaced internal to the outer limiting membrane (in the perinuclear cytoplasm) in many of the accessory cones and rods (Figure 10B,D). They also appeared more metachromatic (pink in color) in toluidine blue stained semi-thin sections (Figure 10B). Besides the appearance of the granules with EM, which indicated they contained glycogen, the granules stained positively with PAS and following treatment with diestase, the PAS staining was no longer observed (data not shown). In contrast, control retinas only had glycogen deposits in the ISs of the accessory cones and rod cells (Figure 10A). In *rge*/*rge* sections, photoreceptor synapses in the OPL were even more disorganized than at earlier ages. The number of discernible ribbons in the OPL in the *rge*/*rge* sections was also even more reduced compared to the younger *rge*/*rge* birds; however, a few could still be observed, and were sometimes very close to the displaced glycogen deposits (data not shown).

*Examination for morphological features of apoptosis:* Despite close examination of sections from *rge*/*rge* retinas at several different ages by light and electron microscopy, no cells displaying morphological features that would indicate they were undergoing apoptosis were seen.

*Immunohistochemistry results (paraffin embedded and frozen sections):* Tyrosine hydroxylase (TH) staining of control retinas was similar to previous reports [25], with TH positive neurites being concentrated at the outer border of the IPL, close to the corresponding amacrine cell body. Additional neurites from these cells can be observed, at a lesser density, branching bilaterally and extending into the IPL close to the

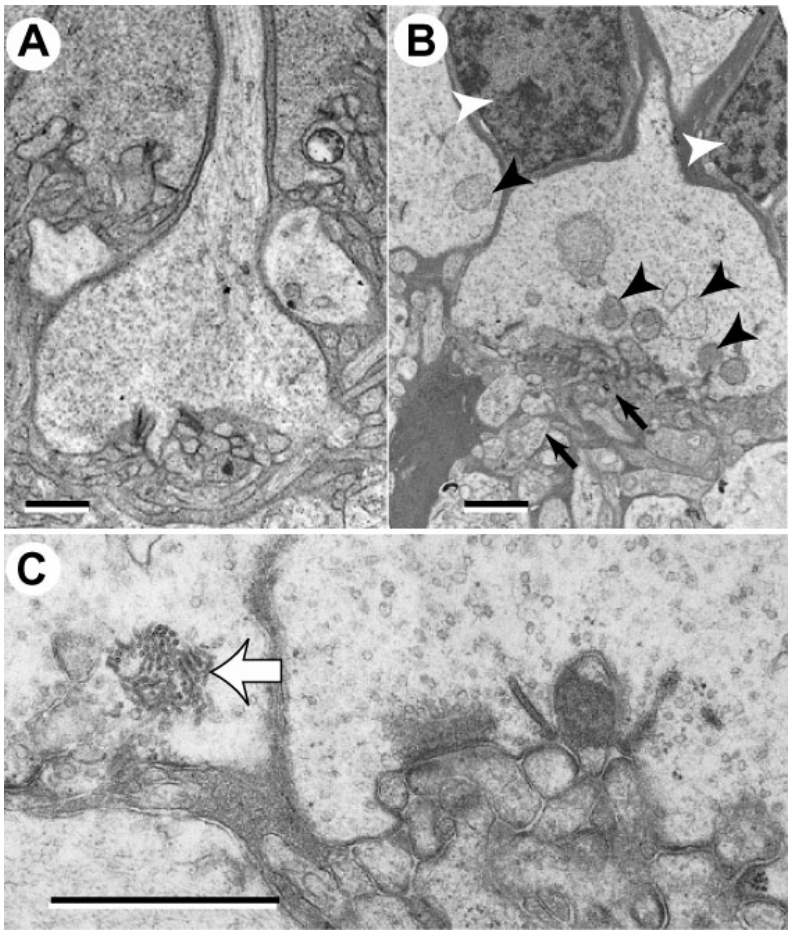


Figure 8. Abnormalities of synaptic terminals. **A** Synaptic terminal of a cone pedicle of a control chick at 7 days of age. **B**: A typical example of a synaptic terminal of a cone pedicle of an *rge*/*rge* chick at 7 days of age. The cytoplasm is less densely stained. Note the disruption in the architecture of the synaptic terminals (small black arrows). Also note the presence of electron dense glial cell bodies separating the photoreceptors (white arrowheads) and multivesicular bodies (black arrowheads). **C**: Higher power detail of an *rge*/*rge* retinal section at 7 days of age demonstrating one of the sets of numerous flattened (tubuliform) vesicles (wide white arrow) in a cone pedicle. Each bar represents 1 μm.

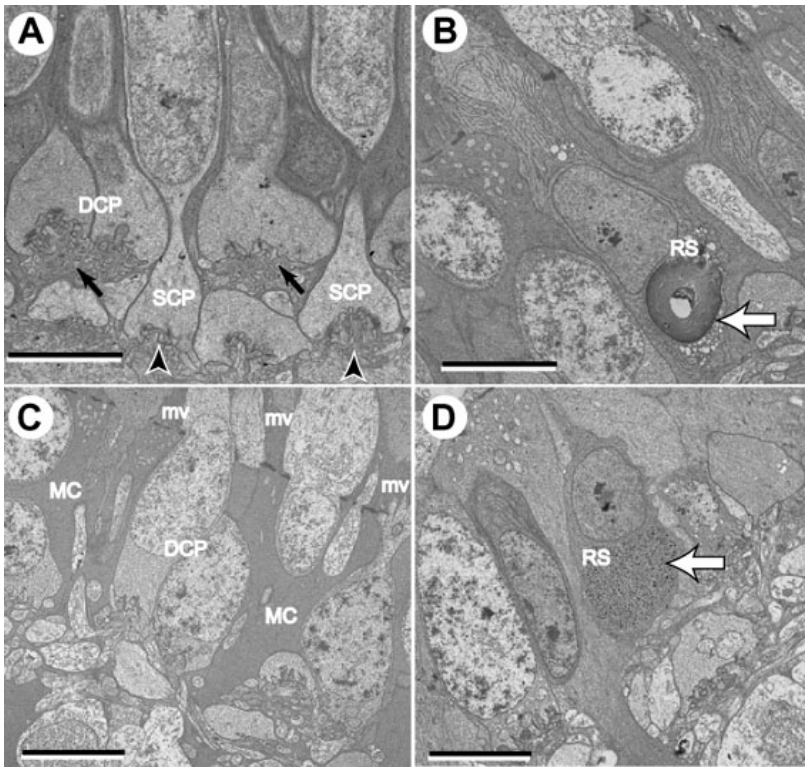


Figure 9. Abnormalities of the outer nuclear layer. Ultra-thin sections of retinal samples from *rge*/*rge* and control birds at 60 days of age. **A**: Note the aspect of the normal chick OPL at 60 days of age. The double cone pedicles terminate in the outer sublayer of the OPL (small black arrows), whereas the single cone pedicles terminate in the inner sublayer (black arrowheads). **B**: Occasionally whorls of membranes forming densely packed stacks of coaxial cylindrical bilayers (myelinoid figures, white arrow) were observed in rod cell bodies in the ONL of *rge*/*rge* birds. **C**: Müller cell processes (MC) occupy gaps between photoreceptors cell bodies. Abundant long Müller cells microvilli (mv) are present between the ISs of the photoreceptor cells. **D**: One large glycogen deposit can be observed in an abnormal location (white arrow). Normally, glycogen can only be found in the ISs. Each bar represent 5 μm. The single cone pedicle (SCP), double cone pedicle (DCP), and rod spherule (RS) are labeled.

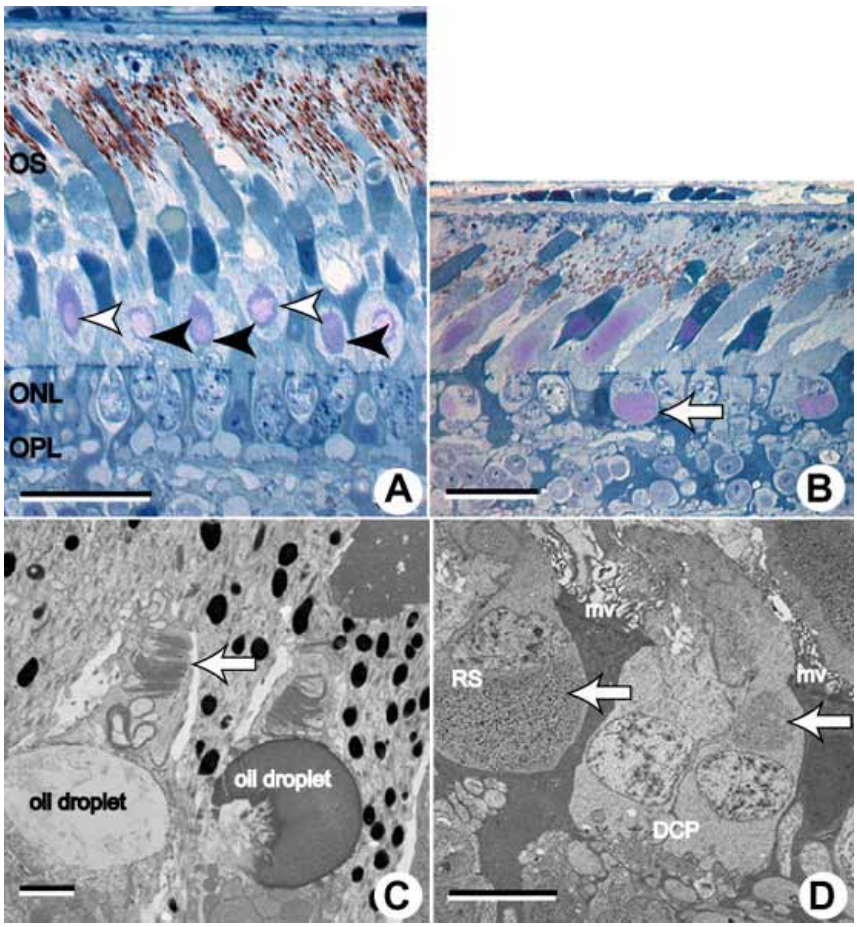


Figure 10. Retinal abnormalities in older birds. Semi-thin sections of retinal samples from *rge*/*rge* and control birds at 270 days of age. **A**: Control retinas show glycogen deposits only in the ISs (external to the outer limiting membrane), which are associated with the rod hyperboloid (white arrowheads) and with the cone accessory cell paraboloid (black arrowheads). The bar represents 20 μm. **B**: Larger glycogen deposits were observed at this age in retinas from *rge*/*rge* birds, that quite often were displaced internal to the outer limiting membrane of the accessory cells of the double cones (arrow). These glycogen deposits are metachromatic in toluidine blue stained semi-thin sections and appear pink in color. The OSs are clearly shorter and disorganized. The bar represents 20 μm. **C**: Ultra-thin section of a retinal sample from an *rge*/*rge* bird demonstrating finer detail of the very short and disorganized cone OSs (arrow). The bar represents 1 μm. **D**: Ultrastructural detail of glycogen deposits (arrows), present in the supranuclear cytoplasm of an accessory cone cell of the double cone pedicle (DCP) and in the subnuclear cytoplasm of a rod cell spherule (RS) of an *rge*/*rge* bird. Long Müller cells microvilli (mv) are abundant between the ISs of the photoreceptor cells of this age group. The bar represents 5 μm. The outer segments (OS), outer nuclear layer (ONL), and outer plexiform layer (OPL) are labeled.

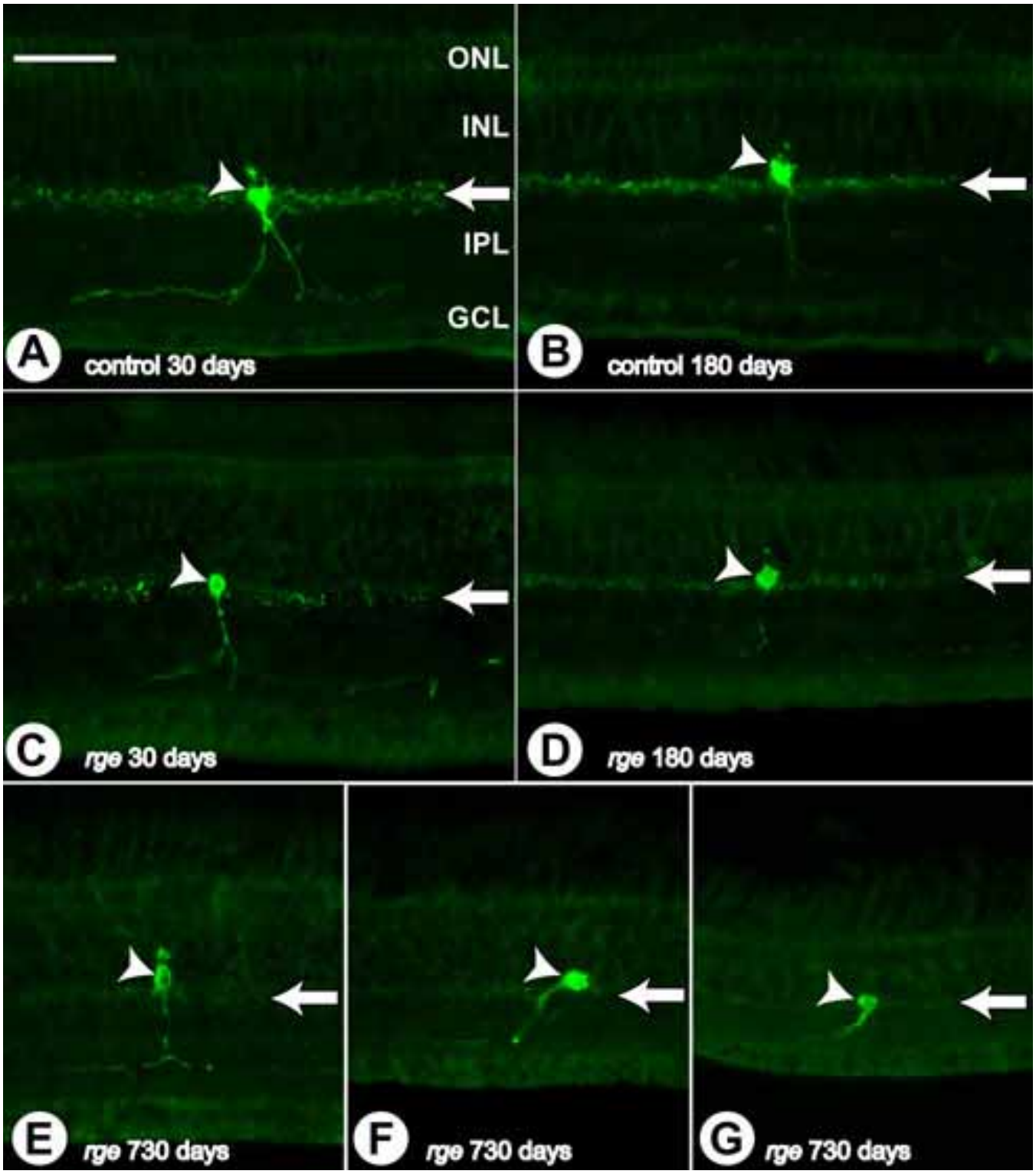


Figure 11. Abnormalities in tyrosine hydroxylase immunohistochemistry. Immunohistochemistry sections using tyrosine hydroxylase (TH) antibody performed on samples from *rge*/*rge* and control birds at 30, 180, and 730 days of age. **A**: Control bird at 30 days of age. **B**: Control bird at 180 days of age. **C**: *rge*/*rge* bird at 30 days of age. **D**: *rge*/*rge* bird at 180 days of age. **E**: Central retina of *rge*/*rge* bird at 730 days of age. **F**: Peripheral retina. **G**: Far peripheral retina. Note that in control retinas, TH positive neurites are found concentrated at the outer border of the IPL, close to the corresponding amacrine cell body. Further neurites from these cells can be observed, at a lesser density, branching bilaterally and extending into the IPL close to the GCL. At later stages of development (180 and 730 days of age) there is an obvious decrease in the density of TH positive neurites in retinal samples from *rge*/*rge* birds (compare **A**,**B** with **C**,**D**; arrows). However, no loss of TH positive somata was observed even at very late stages of the disease (**E**,**F**,**G**; arrowheads). The outer nuclear layer (ONL), inner nuclear layer (INL), inner plexiform layer (IPL), and ganglion cell layer (GCL) are labeled in **A** The bar represents 50 μm.

GCL. In *rge*/*rge* retinas, the basic amacrine cell morphology revealed by TH staining was intact at all ages examined (up to 730 days of age). However, in older *rge*/*rge* birds there was an obvious decrease in the density of TH positive dendrites (Figure 11E-G).

Staining using the monoclonal antibody against mouse opsin (Lab Vision, Fremont, CA) or the mouse anti-rhodopsin antibody (rho4D2) was specific for rod photoreceptors and weakly stained the ISs and strongly stained the OSs in *rge*/*rge* and control birds (Figure 12). The pattern of rhodopsin labeling, however, was abnormal in *rge*/*rge* birds. An increased amount of rhodopsin immunoreactivity was present in the ISs of *rge*/*rge* sections, compared to controls from 13 days of age (Figure 12A,B). This pattern of labeling was more pronounced in peripheral regions of the retina. In sections from older *rge*/*rge* birds (e.g., 180 and 270 days of age) rod OSs appeared swollen, with loss of the normal architecture and organization, this was also more pronounced in the periphery of the retina. Immunoreactivity to both these antibodies was mislocalized to the ONL/OPL region in retinal sections from older *rge*/*rge* birds (Figure 12D,F).

Retinas from *rge*/*rge* chicks showed microglial and glial activation and active phagocytosis when probed with antibodies to RCA-1, GFAP and LEP-100. RCA-1 is a lectin that labels activated microglia in the avian retina [26,27]. The distribution and morphology of microglia positive for RCA-1 observed in the retina of control birds was similar to that previously described [26,27]. In brief, the majority of RCA-1 positive microglia in the normal retina are in the IPL and OPL, although some microglial bodies are also present in the NFL and GCL. In the case of the NFL, RCA-1 positive microglia are more common in the region adjacent to the optic disc. Microglia were ramified through the width of these layers, bearing radial and horizontal processes (Figure 13A). No microglia were found in the photoreceptor layer (Figure 13A). No morphological changes of the microglia were detected at 13 days of age in *rge*/*rge* retinas (Figure 13B). However, by 33 days of age, there were activated microglia present in the IPL and OPL. They were amoeboid shaped cells with enlarged somata (Figure 13C). By 92 days of age, many somata of amoeboid microglia were present in the NFL and INL. These cells had short, stout processes extending from the somata, which suggests that they were highly active at that time. Furthermore, RCA-1 labeled cells were present in the photoreceptor layer of *rge*/*rge* birds at 92 days of age, again suggesting that microglia were highly active in most retinal layers at this age (Figure 13D-F). Müller cells appeared to have increased levels of expression of GFAP in *rge*/*rge* retinas by 30

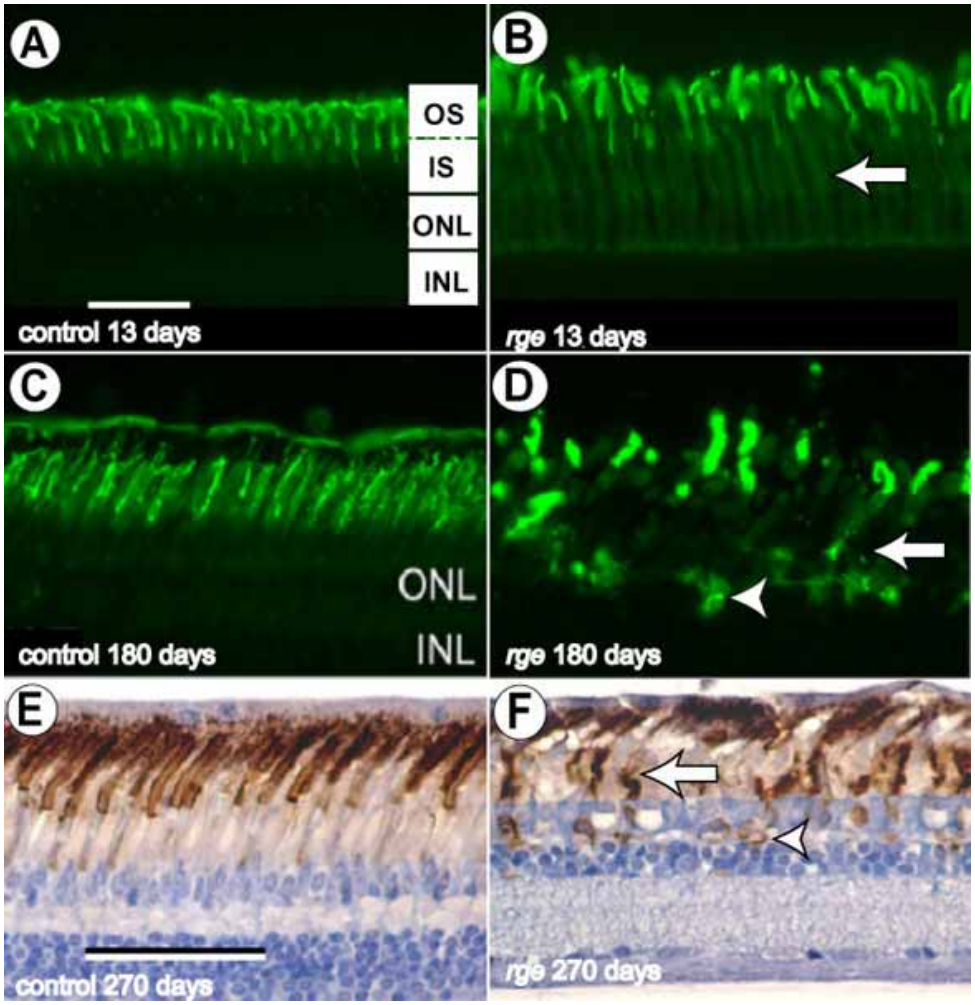


Figure 12. Abnormalities in opsin immunohistochemistry. Fluorescence photomicrographs (**A-D**) and conventional photomicrograph using brown chromogen (**E**,**F**) from immunohistochemistry sections using mouse anti-rhodopsin (**A-D**) and monoclonal antibody against mouse opsin (**E**,**F**). Sections from the mid-periphery of the retina from a control (**A**) and an *rge*/*rge* bird (**B**), at 13 days of age; from a control (**C**) and *rge*/*rge* bird (**D**), at 180 days of age, and from a control (**E**) and *rge*/*rge* bird (**F**), at 270 days of age. Note the presence of increasing amounts of rhodopsin immunoreactivity in the inner segments (IS) of the *rge*/*rge* samples (white arrows on **B**,**D**,**F**). Note that the opsin labeling in the ISs of control samples is minimal (**A**,**C**,**E**). Also, note that, compared to controls (**C**,**E**), the rod outer segments (OS) in the *rge*/*rge* retinas of older birds (**D**,**F**) appear swollen, with loss of the normal architecture and organization. The OSs of *rge*/*rge* chicks also appeared more widely spaced in comparison to the controls. Mislocalization of opsin is present in *rge*/*rge* retinal samples at the outer nuclear layer (ONL)/outer plexiform layer (OPL) level (white arrowheads on **D**,**F**). The inner nuclear layer (INL) is also labeled. The bars represents 50 μm.

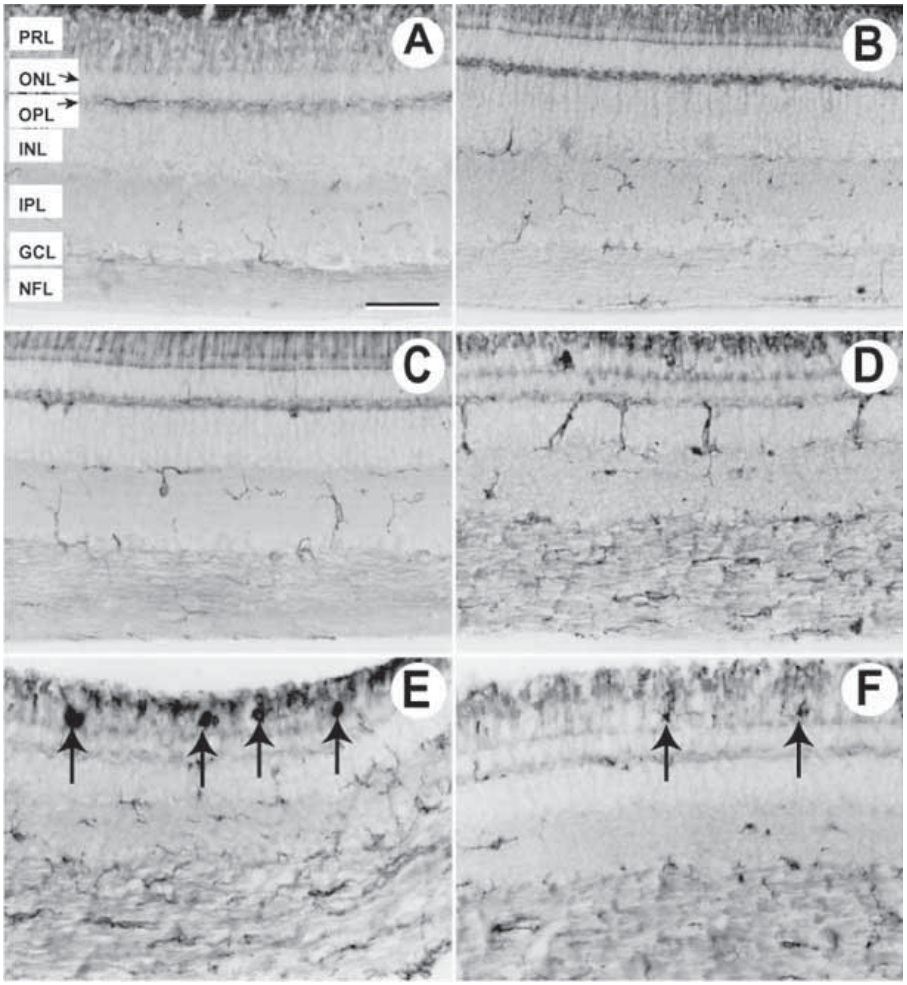


Figure 13. Abnormalities in RCA-1 immunohistochemistry. Immunohistochemically stained retinal sections using RCA-1 antibody of control (**A**) and *rge*/*rge* chicks at 13 days (**B**), 33 days (**C**), and 92 days (**D**-**F**) of age. **A**: Most ramified microglia are located in the nerve fiber layer (NFL), inner plexiform layer (IPL) and outer plexiform layer (OPL). There was no significant difference in microglial morphology between control and *rge*/*rge* retinas at 13 days of age. **C**: In *rge*/*rge* retinas from 33 day old chicks, some microglia in IPL and OPL showed amoeboid shape indicating activation of these cells. (**D**-**F**) Retinal samples from *rge*/*rge* birds at 92 days of age. Note many amoeboid microglia with stout processes are seen in INL and NFL (**D**) and RCA-1 labeled cells similar to macrophages (**E**) or microglia (**F**) were present in the photoreceptor layer (black arrows). The bar represents 50 μm. The photoreceptor layer (PRL), outer nuclear layer (ONL), inner nuclear layer (INL), and ganglion cell layer (GCL) are labeled.

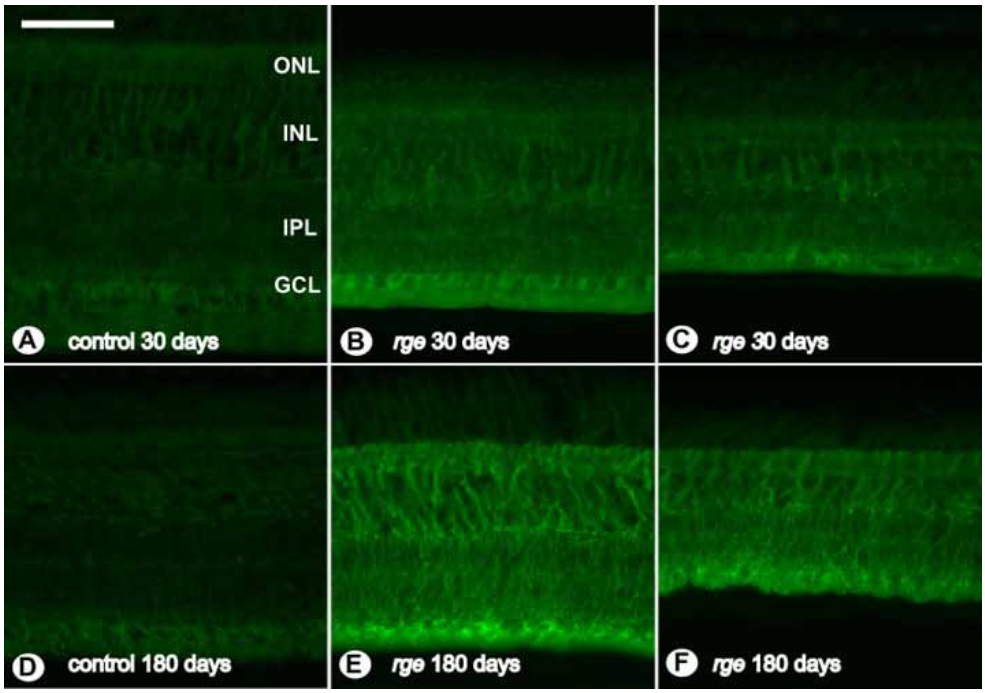


Figure 14. Abnormalities in GFAP immunohistochemistry. GFAP immunohistochemistry staining of sections from retinal samples. **A**: Control bird at 30 days of age. **B**: *rge*/*rge* chick at 30 days of age. **C**: Peripheral retina of an *rge*/*rge* chick at 30 days of age. **D**: Control bird at 180 days of age. **E**: *rge*/*rge* bird at 180 days of age. **F**: Peripheral retina of an *rge*/*rge* bird at 180 days of age. Note the *rge*/*rge* retinas appear to have a progressive increase of GFAP expression, indicating that glial cells (Müller cells) are reactive. The bar represents 50 μm. The outer nuclear layer (ONL), inner nuclear layer (INL), inner plexiform layer (IPL), and ganglion cell layer (GCL) are labeled.

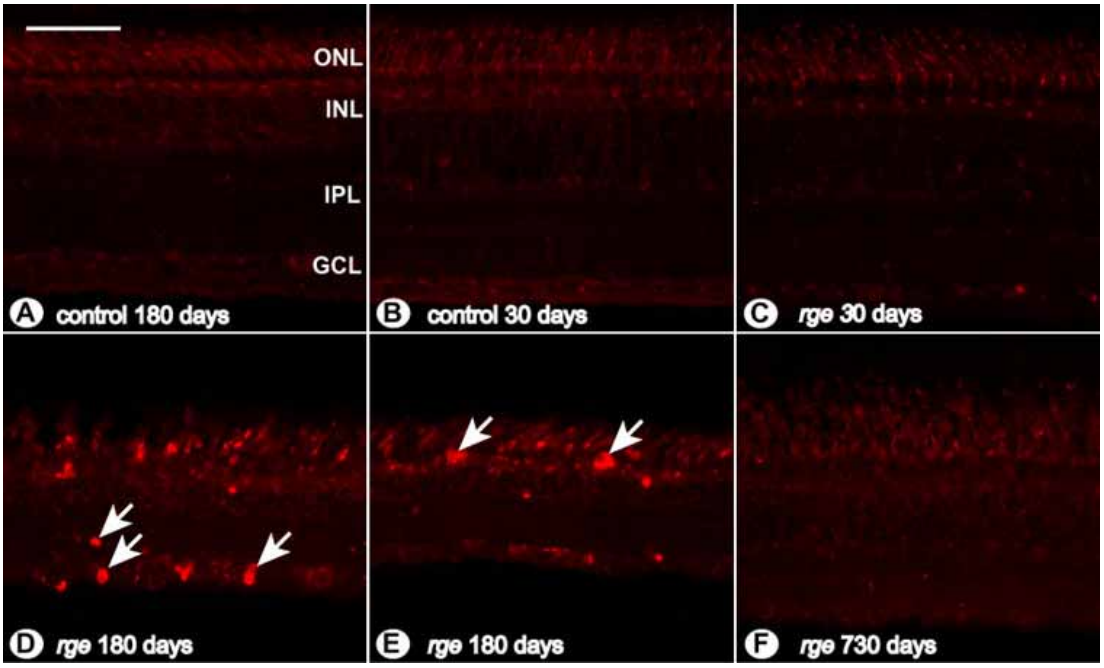


Figure 15. Abnormalities of LEP-100 immunohistochemistry. LEP-100 immunohistochemistry staining of sections from retinal samples. **A**: Retinal section from a control bird at 180 days of age. **B**: Control chick at 30 days of age. **C**: *rge*/*rge* chick at 30 days of age. **D**: Mid-peripheral retinal section of an *rge*/*rge* bird at 180 days of age. **E**: Far-peripheral retina of an *rge*/*rge* bird at 180 days of age. **F**: Central retinal section of an *rge*/*rge* bird at 730 days of age. Note the difference between *rge*/*rge* (**C**,**D**,**E**) and control (**A**,**B**) samples. Several layers of the *rge*/*rge* retinas, mainly outer nuclear layer (ONL), inner nuclear layer (INL), inner plexiform layer (IPL), and ganglion cell layer (GCL) at 180 days of age were positively stained for this antibody (white arrows). At 30 days and 730 days of age, no differences could be detected between *rge*/*rge* and control samples. The bar represents 50 μm.

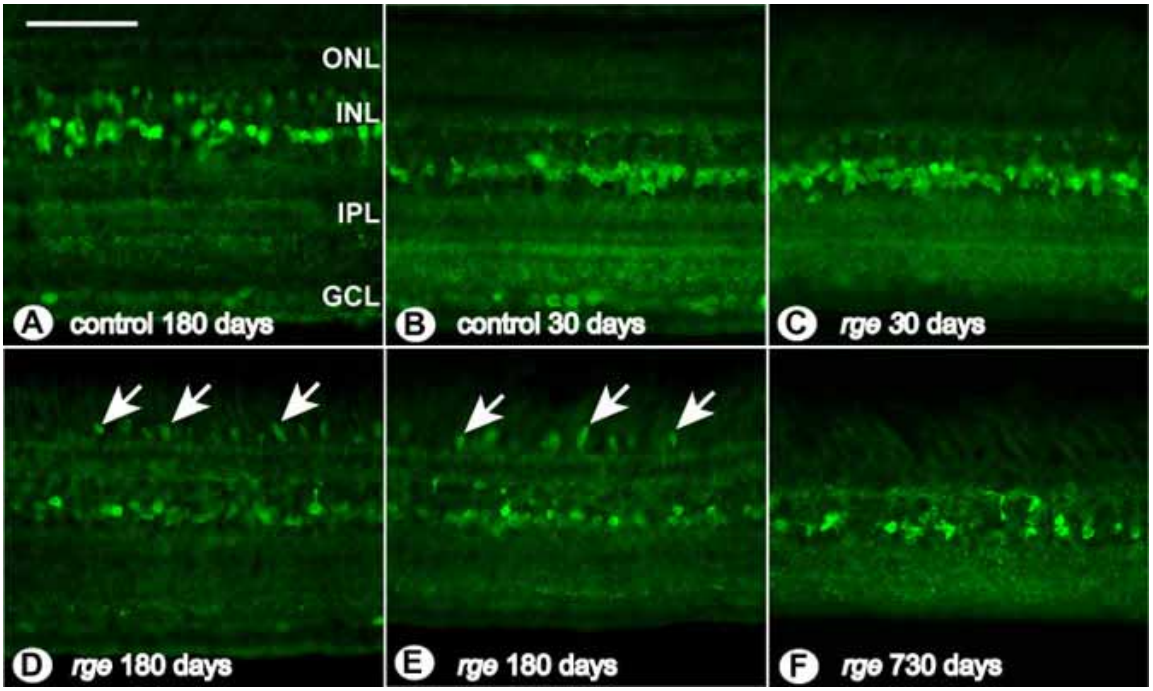


Figure 16. Abnormalities in glycine immunohistochemistry. Glycine immunohistochemistry of sections from retinal samples. **A**: Control bird at 180 days of age. **B**: control chick at 30 days of age. **C**: *rge*/*rge* bird at 30 days of age. **D**: *rge*/*rge* chick at 180 days of age (central area of the retina). **E**: Retinal section from an *rge*/*rge* bird at 180 days of age (periphery of the retina). **F**: Retinal section of an *rge*/*rge* bird at 730 days of age. Note the glycine immunoreactive "blobs" (arrows) detected in the ISs of some photoreceptors in retinas from older *rge*/*rge* birds (**D**,**E**). The bar represents 50 μm. The outer nuclear layer (ONL), inner nuclear layer (INL), inner plexiform layer (IPL), and ganglion cell layer (GCL) are labeled.

days of age, indicating that these glial cells were reactive (Figure 14). However, by 730 days of age, no difference was observed between *rge*/*rge* and control retinas for GFAP positive cells. Retinas from 730 day old birds are not shown here. Staining using the LEP-100 antibody showed differences between *rge*/*rge* and control retinas. The LEP-100 antibody recognizes a lysosomal glycoprotein that is only present in cells that are actively phagocytic. In *rge*/*rge* retinas, activated phagocytes were detected in all layers of the retina at 180 days of age, while these cells were not detected at the other ages studied (30 and 730 days of age). Therefore, controls, 30 day, and 730 day old *rge*/*rge* retinas had no activated phagocytes (Figure 15).

Glycine immunoreactive "blobs" were detected mainly in the ISs of some photoreceptors in the *rge*/*rge* retinas (Figure 16). These glycine immunoreactive blobs may have been the large glycogen deposits that accumulated in the ISs of photoreceptors of *rge*/*rge* birds.

The staining for synaptic vesicle protein 2 (SV2), a ubiquitously expressed synaptic vesicle protein, revealed abnormalities in the stratification of the OPL in the *rge*/*rge* birds compared to controls, substantiating the results observed ultrastructurally. Control retinas stained with SV2 showed an organized bilayered pattern of labeling in the OPL. *rge*/*rge* retinas lacked the organized stratification of the OPL, and instead showed a single intensely immunoreactive layer in the OPL (figure not shown).

In analyzing samples that were immunocytochemically stained for visinin, only a mild distortion in the normal arrangement and a mild loss of reactivity could be observed at 180 and 730 days of age in *rge*/*rge* retinas (figure not shown).

The following antibodies showed no difference in labeling pattern, distribution or the amount of positive cells between control and *rge*/*rge* retinas: TfBP, GCAP1, VAMP1, GABA-A, caspase 3, β3-tubulin, glucagon, neurofilament, vimentin, Hu, Islet1, or TrkA.

*TUNEL Staining:* No TUNEL positive cells were detected in retinal sections from *rge*/*rge* or control birds. The lack of TUNEL staining is in keeping with the results of caspase 3 staining and the results of examination for morphological features of apoptosis.

## DISCUSSION

The vision of *rge*/*rge* chicks deteriorates over the first few weeks after hatch and is poorer under lower lighting conditions. Approximately 30 days after hatch vision has deteriorated to such an extent that the *rge*/*rge* chicks are functionally blind. Intriguingly, examination by light microscopy reveals that the retinal morphology in the *rge*/*rge* retinal sections is remarkably preserved in spite of the loss of vision. Later in the disease, ossification of the entire retina and focal linear areas of photoreceptor disorganization have been previously described in some affected birds [16-18]. Both are believed to be secondary retinal changes that occur after functional visual abnormalities and globe enlargement occur [18].

The results from this study revealed several abnormalities in different retinal regions of the *rge*/*rge* birds. The earliest changes detected were in the OPL. The photoreceptor synaptic terminal organization in the *rge*/*rge* birds appeared to be disrupted with loss of the normal regular bilayered arrangement seen in control birds and distortion of the photoreceptor pedicles and spherules. These changes became more severe as the disease progressed. The synaptic terminals also appeared to have fewer synaptic ribbons. The remaining ribbons were usually larger, more electrolucent and contained abnormally shaped synaptic vesicles. The ER was frequently located within the photoreceptor cell bodies rather than in the ISs, particularly in accessory cells of the double cones. Abnormal localization and progressive accumulation of glycogen occurred in the photoreceptor perinuclear region of *rge*/*rge* chicks associated with the abnormally located ER. This led to large glycogen deposits very close to the nucleus and synaptic area in older *rge*/*rge* birds. This glycogen accumulation and mislocalization was not associated with lysosomal membranes as in the case with glycogen accumulation observed in retinal glycogenosis, where the glycogen accumulation is present in most cell types in the retina and always associated with lysosomes [28]. Additionally in the older affected birds myelinoid bodies (also called myeloid bodies), which are whorls of concentric layers of cell membranes, developed in the photoreceptors between the nucleus and the synaptic terminal. One suggestion for the development of myelinoid bodies is degeneration of ER [29], however the link between the myelinoid bodies and abnormal location of ER with associated glycogen accumulation is not clear. The glycine positive "blobs" that were present in the *rge*/*rge* retinas were glycine accumulations in the ISs of some photoreceptors. This may indicate abnormal photoreceptor metabolism.

The morphological abnormalities in the photoreceptor synaptic terminals might reflect abnormal physiological function and could underlie the vision loss that occurs in the *rge*/*rge* birds in the absence of marked photoreceptor cell loss. The vesicular changes observed in the synapses, along with the apparently less numerous ribbons, might suggest a defect in the vesicle formation machinery, or a defect in the exocytosis docking mechanism. The presence of abnormal synaptic vesicles along with the morphological changes observed in the photoreceptor pedicles of *rge*/*rge* birds are somewhat similar to the ones observed in the photoreceptor synapses of synaptophysin knockout mouse [30] and in the *rdgE* (Drosophila retinal degeneration E) [31]. Both the mutant mouse and fly exhibited a number of synaptic and vesicular defects, including a buildup of very large multivesicular bodies, and an increased amount of rough endoplasmic reticulum.

The previously reported early reduction in dim light vision in *rge*/*rge* birds suggests that rod dysfunction precedes loss of cone mediated vision [18]. Opsin immunohistochemistry showed abnormalities in rods from 13 days of age. Initially there was increased opsin immunoreactivity in the ISs and later mislocalization to the ONL. Furthermore, there was a progressive decrease in the number of rod OSs per unit length of retina with age. Abnormal trafficking of opsin in damaged or abnormal rods has been observed in other forms of inherited retinal degenerations, such as in people suffering from

retinitis pigmentosa and in the tulp1$^{-/-}$ mice [32-34]. As the disease progressed the *rge*/*rge* chicks developed a generalized shortening and disorganization of all photoreceptor OSs.

The results from the retinal thickness measurements show *rge*/*rge* birds develop a progressive retinal thinning. Initially the ventral regions and far dorsal peripheral regions of the retina suffered the greatest reduction in thickness. This is possibly a direct consequence of globe stretch caused by the globe enlargement that occurs, initially in a radial direction [18] and this has a greater effect at the equator of the globe. At later stages a generalized thinning of all retinal layers occurs. In the early stages of the disease, the greatest decrease in thickness occurred in the inner retina. Ganglion cells, however, were not decreased in number per unit retinal length in spite of the retinal stretch. Markers used for amacrine and horizontal cells showed that the numbers of these two cell populations were maintained. The decrease in TH positive dendrites from amacrine cells may have resulted from retinal stretch caused by the increased globe enlargement. Previous studies have shown that where there is increased ocular growth and passive retinal stretch the density of TH positive amacrine cells decreases while total cell numbers within the retina remain constant [35]. In retinas from *rge*/*rge* birds, the TH positive cells do not appear to sprout additional neurites to maintain a constant density of dendrites during the retinal stretch that occurs. Whereas in experimentally induced retinal stretch, the density of TH positive dendrites is maintained [35]. This finding suggests that the *rge*/*rge* phenotype includes the inability of some types of amacrine cells to sprout dendrites. While TH and glucagon containing amacrine cells have been implicated in regulating the overall growth of the eye [36,37], these cell types are present in affected birds showing that globe enlargement is not secondary to their loss. It has previously been shown that amacrine cell death is one cause of globe enlargement [24,38].

In the later stages of the disease, marked gliosis develops. Glial processes occupied spaces in the OPL where normally pedicles and spherules would have been located and they also filled gaps between the somata of photoreceptor cells. This glial activation is reflected by increased GFAP and RCA-1 staining (indicating activated glial and microglial cells). Atrophy and gliosis of the inner retinal layers internal to the outer plexiform layer was also previously observed in the *rge*/*rge* retinas by another group of researchers [17]. It is not clear whether the gliosis development is in response to the development of gaps between cells, is triggered by the progressive retinal stretch, or is due to spaces caused by a disease associated injury and loss of retinal cells. The increased immunoreactivity to LEP-100 in the *rge*/*rge* retina suggests the presence of activated phagocytes. These phagocytes may have been activated by growth factors and cytokines that could be somehow elevated in the retinas from *rge*/*rge* birds. Judging by the different sizes and morphology of the LEP-100 positive cells, some of these cells appear to be macrophages that have migrated into the retina, while others might be activated resident microglia. Alternatively, microglia may have been activated by primary photoreceptor cell death, similar to what happens in human retinas with retinitis pigmentosa [39].

No morphological (LM or EM), immunocytochemical (caspase 3) or molecular (TUNEL) evidence of apoptosis was detected. It seems likely that cell loss in the *rge*/*rge* retina occurs gradually. By 730 days of age no difference could be detected between *rge*/*rge* and control sections for GFAP and LEP-100 immunostaining, indicating that most of the glial activation and possibly phagocytosis have been terminated by that point.

The *rge*/*rge* phenotype appears unique with morphological features quite unlike those described in the other forms of chicken retinal dystrophies such as *rd*, *rdd*, *dam*, and *beg* [12-14,40-44]. Although ERG responses in the young *rge*/*rge* chick show supernormal b-wave amplitudes to brighter light stimuli [18] and a similar ERG abnormality is present in mice and humans with NR2E3 gene mutations [20,45,46], morphologically the diseases are quite different. Unlike the NR2E3 mutant mice and humans, where S-cone photoreceptors are present at greatly increased numbers, in the *rge*/*rge* chicken, there were no obvious changes in photoreceptor populations. Molecular genetic studies to identify the causal gene mutation should help explain why the morphological features of the *rge*/*rge* phenotype develop and clarify the association with the vision loss and the electroretinographic abnormalities.

## REFERENCES

1. Keep JM. Clinical aspects of progressive retinal atrophy in the Cardigan Welsh Corgi. Aust Vet J 1972; 48:197-9.
2. Blanks JC, Adinolfi AM, Lolley RN. Photoreceptor degeneration and synaptogenesis in retinal-degenerative (rd) mice. J Comp Neurol 1974; 156:95-106.
3. Aguirre GD, Rubin LF. Rod-cone dysplasia (progressive retinal atrophy) in Irish setters. J Am Vet Med Assoc 1975; 166:157-64.
4. Bowes C, Li T, Danciger M, Baxter LC, Applebury ML, Farber DB. Retinal degeneration in the rd mouse is caused by a defect in the beta subunit of rod cGMP-phosphodiesterase. Nature 1990; 347:677-80.
5. Petersen-Jones SM, Entz DD, Sargan DR. cGMP phosphodiesterase-alpha mutation causes progressive retinal atrophy in the Cardigan Welsh corgi dog. Invest Ophthalmol Vis Sci 1999; 40:1637-44.
6. Petersen-Jones SM, Khan NW, Tuntivanich N. Electroretinographic features of the PDE6A mutant dog. ARVO Annual Meeting; 2003 May 4-9; Fort Lauderdale, FL.
7. Aguirre G, Alligood J, O'Brien P, Buyukmihci N. Pathogenesis of progressive rod-cone degeneration in miniature poodles. Invest Ophthalmol Vis Sci 1982; 23:610-30.
8. Narfstrom K, Wrigstad A. Clinical, electrophysiological and morphological changes in a case of hereditary retinal degeneration in the Papillon dog. Vet Ophthalmol 1999; 2:67-74.
9. Sandberg MA, Pawlyk BS, Berson EL. Full-field electroretinograms in miniature poodles with progressive rod-cone degeneration. Invest Ophthalmol Vis Sci 1986; 27:1179-84.
10. Pardue MT, McCall MA, LaVail MM, Gregg RG, Peachey NS. A naturally occurring mouse model of X-linked congenital stationary night blindness. Invest Ophthalmol Vis Sci 1998; 39:2443-9.
11. Narfstrom K, Wrigstad A, Nilsson SE. The Briard dog: a new animal model of congenital stationary night blindness. Br J

Ophthalmol 1989; 73:750-6.
12. Semple-Rowland SL, Lee NR, Van Hooser JP, Palczewski K, Baehr W. A null mutation in the photoreceptor guanylate cyclase gene causes the retinal degeneration chicken phenotype. Proc Natl Acad Sci U S A 1998; 95:1271-6.
13. Pollock BJ, Wilson MA, Randall CJ, Clayton RM. Preliminary observations of a new blind chick mutant (beg). In: Clayton RM, Reading HW, Haywood J, Wright A, editors. Problems of normal and genetically abnormal retinas. London: Academic Press; 1982. p. 241-7.
14. Randall CJ, Wilson MA, Pollock BJ, Clayton RM, Ross AS, Bard JB, McLachlan I. Partial retinal dysplasia and subsequent degeneration in a mutant strain of domestic fowl (rdd). Exp Eye Res 1983; 37:337-47.
15. Curtis PE, Baker JR, Curtis R, Johnston A. Impaired vision in chickens associated with retinal defects. Vet Rec 1987; 120:113-4.
16. Curtis R, Baker JR, Curtis PE, Johnston A. An inherited retinopathy in commercial breeding chickens. Avian Pathol 1988; 17:87-99.
17. Inglehearn CF, Morrice DR, Lester DH, Robertson GW, Mohamed MD, Simmons I, Downey LM, Thaung C, Bridges LR, Paton IR, Smith J, Petersen-Jones S, Hocking PM, Burt DW. Genetic, ophthalmic, morphometric and histopathological analysis of the Retinopathy Globe Enlarged (rge) chicken. Mol Vis 2003; 9:295-300 .
18. Montiani-Ferreira F, Li T, Kiupel M, Howland H, Hocking P, Curtis R, Petersen-Jones S. Clinical features of the retinopathy, globe enlarged (rge) chick phenotype. Vision Res 2003; 43:2009-18.
19. Jurklies B, Weismann M, Kellner U, Zrenner E, Bornfeld N. [Clinical findings in autosomal recessive syndrome of blue cone hypersensitivity.] Ophthalmologe 2001; 98:285-93.
20. Milam AH, Rose L, Cideciyan AV, Barakat MR, Tang WX, Gupta N, Aleman TS, Wright AF, Stone EM, Sheffield VC, Jacobson SG. The nuclear receptor NR2E3 plays a role in human retinal photoreceptor differentiation and degeneration. Proc Natl Acad Sci U S A 2002; 99:473-8.
21. Gomez A, Cedano J, Oliva B, Pinol J, Querol E. The gene causing the Best's macular dystrophy (BMD) encodes a putative ion exchanger. DNA Seq 2001; 12:431-5.
22. Humayun MS, Prince M, de Juan E Jr, Barron Y, Moskowitz M, Klock IB, Milam AH. Morphometric analysis of the extramacular retina from postmortem eyes with retinitis pigmentosa. Invest Ophthalmol Vis Sci 1999; 40:143-8.
23. Hacker G. The morphology of apoptosis. Cell Tissue Res 2000; 301:5-17.
24. Fischer AJ, Seltner RL, Poon J, Stell WK. Immunocytochemical characterization of quisqualic acid- and N-methyl-D-aspartate-induced excitotoxicity in the retina of chicks. J Comp Neurol 1998; 393:1-15.
25. Ballesta J, Terenghi G, Thibault J, Polak JM. Putative dopamine-containing cells in the retina of seven species demonstrated by tyrosine hydroxylase immunocytochemistry. Neuroscience 1984; 12:1147-56.
26. Navascues J, Moujahid A, Quesada A, Cuadros MA. Microglia in the avian retina: immunocytochemical demonstration in the adult quail. J Comp Neurol 1994; 350:171-86.
27. Won MH, Kang TC, Cho SS. Glial cells in the bird retina: immunochemical detection. Microsc Res Tech 2000; 50:151-60.
28. Goebel HH, Kohlschutter A, Pilz H. Ultrastructural observations on the retina in type II glycogenosis (Pompe's disease). Ophthalmologica 1978; 176:61-8.
29. Stevenson GW, Kiupel M, Mittal SK, Kanitz CL. Ultrastructure of porcine circovirus in persistently infected PK-15 cells. Vet Pathol 1999; 36:368-78.
30. Spiwoks-Becker I, Vollrath L, Seeliger MW, Jaissle G, Eshkind LG, Leube RE. Synaptic vesicle alterations in rod photoreceptors of synaptophysin-deficient mice. Neuroscience 2001; 107:127-42.
31. Zars T, Hyde DR. rdgE: a novel retinal degeneration mutation in Drosophila melanogaster. Genetics 1996; 144:127-38.
32. Li ZY, Kljavin IJ, Milam AH. Rod photoreceptor neurite sprouting in retinitis pigmentosa. J Neurosci 1995; 15:5429-38.
33. Hagstrom SA, Duyao M, North MA, Li T. Retinal degeneration in tulp1-/- mice: vesicular accumulation in the interphotoreceptor matrix. Invest Ophthalmol Vis Sci 1999; 40:2795-802.
34. Gao J, Cheon K, Nusinowitz S, Liu Q, Bei D, Atkins K, Azimi A, Daiger SP, Farber DB, Heckenlively JR, Pierce EA, Sullivan LS, Zuo J. Progressive photoreceptor degeneration, outer segment dysplasia, and rhodopsin mislocalization in mice with targeted disruption of the retinitis pigmentosa-1 (Rp1) gene. Proc Natl Acad Sci U S A 2002; 99:5698-703.
35. Teakle EM, Wildsoet CF, Vaney DI. The spatial organization of tyrosine hydroxylase-immunoreactive amacrine cells in the chicken retina and the consequences of myopia. Vision Res 1993; 33:2383-96.
36. Fischer AJ, McGuire JJ, Schaeffel F, Stell WK. Light- and focus-dependent expression of the transcription factor ZENK in the chick retina. Nat Neurosci 1999; 2:706-12.
37. Iuvone PM, Tigges M, Stone RA, Lambert S, Laties AM. Effects of apomorphine, a dopamine receptor agonist, on ocular refraction and axial elongation in a primate model of myopia. Invest Ophthalmol Vis Sci 1991; 32:1674-7.
38. Feldkaemper MP, Schaeffel F. Evidence for a potential role of glucagon during eye growth regulation in chicks. Vis Neurosci 2002; 19:755-66.
39. Gupta N, Brown KE, Milam AH. Activated microglia in human retinitis pigmentosa, late-onset retinal degeneration, and age-related macular degeneration. Exp Eye Res 2003; 76:463-71.
40. Smyth JR Jr, Boissy RE, Fite KV, Albert DM. Retinal dystrophy associated with a postnatal amelanosis in the chicken. Invest Ophthalmol Vis Sci 1981; 20:799-803.
41. Fulton AB, Fite KV, Bengston L. Retinal degeneration in the delayed amelanotic (DAM) chicken: an electroretinographic study. Curr Eye Res 1982-83; 2:757-63.
42. Burt DW, Morrice DR, Lester DH, Robertson GW, Mohamed MD, Simmons I, Downey LM, Thaung C, Bridges LR, Paton IR, Gentle M, Smith J, Hocking PM, Inglehearn CF. Analysis of the rdd locus in chicken: a model for human retinitis pigmentosa. Mol Vis 2003; 9:164-70 .
43. Ulshafer RJ, Allen C, Dawson WW, Wolf ED. Hereditary retinal degeneration in the Rhode Island Red chicken. I. Histology and ERG. Exp Eye Res 1984; 39:125-35.
44. Ulshafer RJ, Allen CB. Hereditary retinal degeneration in the Rhode Island Red chicken: ultrastructural analysis. Exp Eye Res 1985; 40:865-77.
45. Akhmedov NB, Piriev NI, Chang B, Rapoport AL, Hawes NL, Nishina PM, Nusinowitz S, Heckenlively JR, Roderick TH, Kozak CA, Danciger M, Davisson MT, Farber DB. A deletion in a photoreceptor-specific nuclear receptor mRNA causes retinal degeneration in the rd7 mouse. Proc Natl Acad Sci U S A 2000; 97:5551-6.
46. Haider NB, Jacobson SG, Cideciyan AV, Swiderski R, Streb LM, Searby C, Beck G, Hockey R, Hanna DB, Gorman S, Duhl D, Carmi R, Bennett J, Weleber RG, Fishman GA, Wright AF, Stone

EM, Sheffield VC. Mutation of a nuclear receptor gene, NR2E3, causes enhanced S cone syndrome, a disorder of retinal cell fate. Nat Genet 2000; 24:127-31.

The print version of this article was created on 14 Jan 2005. This reflects all typographical corrections and errata to the article through that date. Details of any changes may be found in the online version of the article.